Vietnam Journal of Science and Technology ***63*** *(1) (2025) 63-74*

doi:10.15625/2525-2518/18365

A hydrothermal pathway for TiO_2-rGO heterojunction nanocomposite to enhance hydrogen peroxide evolution

Tong Hoang Lin[1, 2, 3], Le Minh Huong[1, 2, 3], Che Quang Cong[1, 2, 3], Nguyen Thanh Hoai Nam[1, 2, 3], Nguyen Tan Thinh[1, 2, 3], Doan Thi Yen Oanh[4], Nguyen Huu Hieu[1, 2, 3,*]

[1]*VNU-HCM, Key Laboratory of Chemical Engineering and Petroleum Processing (Key CEPP Lab), Ho Chi Minh City University of Technology (HCMUT), 268 Ly Thuong Kiet Street, District 10, Ho Chi Minh City, Viet Nam*

[2]*Faculty of Chemical Engineering, Ho Chi Minh City University of Technology (HCMUT),*

268 Ly Thuong Kiet Street, District 10, Ho Chi Minh City, Viet Nam
[3]*Vietnam National University Ho Chi Minh City (VNU-HCM), Linh Trung Ward, Thu Duc City, Viet Nam*

[4]*Publishing House for Science Technology, Vietnam Academy of Science and Technology, 18 Hoang Quoc Viet, Cau Giay, Ha Noi, Viet Nam*

[*]Email: *nhhieubk@hcmut.edu.vn*

Received: 25 May 2023; Accepted for publication: 9 May 2024

Abstract. In this study, titanium dioxide-reduced graphene oxide (TiO_2-rGO(TGO)) nanocomposite was synthesized via hydrothermal pathway. The characterization of the fabricated material revealed an efficient incorporation of the two constituents, as well as a notable decrease in the band gap energy of TGO compared to that of pristine TiO_2 (2.62 versus 3.15 eV, respectively), which can expand the absorption spectrum of the catalyst towards the visible region. Electrochemical studies also elucidated the contribution of the rGO substrate in prolonging the recombination rate of charge carriers, signifying a noticeable enhancement in the photocatalytic capability of the TGO composite. Meanwhile, the hydrogen peroxide evolution performance of the synthesized photocatalyst was relatively promising with a concentration of up to 158.34 μM after 180 min. Along with further examinations additionally showing the plausible formation and participation of reactive oxygen radicals during the photocatalytic scheme, the TGO material indicates a good potential for several practical applications, especially the generation of hydrogen peroxide under light irradiation.

Keywords: Titanium dioxide, reduced graphene oxide, band gap, hydrogen peroxide.

Classification numbers: 2.1.1.

1. INTRODUCTION

Nowadays, the tremendous advances in technology over the past centuries have remarkably accelerated civilization growth as well as triggered vast industrialization worldwide. Such phenomena resulted in a notable increase in total energy demand and consumption. Thus, the need to discover alternative energy sources is highly essential [1], not only to provide high-

performance energy sinks for the production sector and human life but also to reduce numerous detrimental impacts on the environment due to the exploitation of fossil-derived resources [2]. In recent years, solar light has been reported to be a prominent candidate, which is green and an infinite energy source. It is estimated that the accumulated amount of energy that the sun emits is 3.10^{24} Jannually, which is incredibly a thousand-fold higher than the total human energy consumption [3]. The immense amount of solar energy can currently be utilized as thermal and photovoltaic power plants via some modern devices, which can be remarkably impeded by various factors, namely geological location, time, and local climate [4]. Therefore, the utilization of an excellent photocatalyst to facilely convert solar energy can be suggested as an effective pathway to effectively exploit this renewable power source.

Hydrogen peroxide (H_2O_2), a well-known oxidant that ranks among the most important chemicals in the world [5], is an eco-friendly chemical that can perform favorable oxidation and generate highly active free radicals for bacterial deactivation, signifying a green and effectual disinfectant by releasing only benign products like H_2O and O_2 during its reaction [6]. Furthermore, H_2O_2 can also be deployed not only to clean wounds in medical sterilization at a low concentration (3 %) but also in many fields such as wastewater treatment, paper bleaching, and electronic industry [7, 8]. Thanks to its massive necessity, the annual H_2O_2 production worldwide has now exceeded 4 million tons per year [9] and is anticipated to experience continuous growth over the next few years [10]. Currently, more than 95 % of the H_2O_2 production utilizes the industrial-scale anthraquinone (AQ) technology [11], which requires high energy input while producing large amounts of wastewater due to multi-step oxidation and hydrogenation reactions [12].

On the other hand, among photocatalysts, titanium dioxide (TiO_2) emerges as a potent representative for photocatalytic applicability, owing to its outstanding features: non-toxicity, excellent economic, chemical, and photochemical stabilities. However, bare TiO_2 exhibits some noticeable drawbacks of a wide band gap (~3.15 eV) and a rapid recombination rate of electron-hole pairs [13,14], which provides a good photocatalytic activity only within a narrow ultraviolet (UV) region. The incorporation of TiO_2 with carbon-based supports is a commonly adopted method to additionally promote the photocatalytic efficiency of the composite as a whole. In particular, reduced graphene oxide (rGO), a graphene derivative, endows good electrical conductivity, adsorption capacity, electron mobility, and large specific surface area [15]. Upon the combination with TiO_2, rGO can be anticipated to effectively reduce the recombination rate of electron-hole pairs while increasing the contact surface area between the catalyst and the photons from the light source, eventually resulting in a promoted photocatalytic performance as compared to the pristine TiO_2 semiconductor [16].

In this study, titanium dioxide-reduced graphene oxide (TiO_2-rGO(TGO)) composite was synthesized using a hydrothermal pathway, in which titanium(IV) isopropoxide (TIP) was utilized as the metallic precursor. The characterization of the synthesized materials was conducted by several modern analytical methods. Besides, the photocatalytic capability of the fabricated TGO was subjected to the photo-generation of H_2O_2 under visible light illumination.

2. MATERIALS AND METHODS

2.1. Materials and chemicals

Graphite (Gi), potassium permanganate ($KMnO_4$), phosphoric acid (H_3PO_4), sulfuric acid (H_2SO_4), H_2O_2, isopropyl alcohol (C_3H_7OH (IPA)), acetic acid (CH_3COOH), ethanol (C_2H_5OH),

potassium iodide (KI), TIP, and potassium hydrogen phthalate ($C_8H_5KO_4$(KHP)) were purchased from Sigma Aldrich, USA. All chemicals were of analytical grade and used without further purification. Double-distilled water was used for all experiments.

2.2. Synthesis of TGO

GO was initially prepared using a modified Hummer's method similar to previous reports [17]. Regarding TGO, at first, 50 mL of the mentioned GO suspension was added with a defined amount of TIP, 50 mL of ethanol, and 1 mL of acetic acid, respectively, under ultrasonication for 20 min [18, 19]. Then, the mixture underwent a hydrothermal treatment in a Teflon autoclave at 90 ^oC for 2 h. Lastly, the mixture was thoroughly washed with distilled water several times to remove impurities before being dried at 80 ^oC to form TGO.

2.3. Characterization of materials

FTIR spectroscopy (Bruker TENSOR-27, Germany) was conducted using KBr pellets over a wavelength spectrum of 600 - 4000 cm^{-1} with an accuracy of 0.1 % T and resolution of 0.2 cm^{-1}. XRD diffractograms (Bruker XRD D8, Germany) were recorded via CuK_α irradiation (λ = 0.154 nm) with a scanning region of 2θ = 0 - 80° and a scanning rate of 2 °/min. Raman spectroscopy (LabRam micro-Raman) was carried out at an excitation wavelength of 632 nm using a He-Ne laser. SEM micrographs (Hitachi S4800, Japan) were performed at a voltage of 10 kV and a magnification scale of x5000, whilst EDS analysis (Jeol JMS 6490, Japan) was conducted to examine the composition of three major elements, namely C, O, and Ti, in the surveyed samples. For the electrochemical measurements, EIS and CV curves were recorded using a three-electrode system, namely a working electrode, a Pt counter electrode, and a reference electrode ($Hg/HgCl_2$), in PBS electrolyte on an electrochemical workstation (CH Instrument 760D) [20]. In which, the surveyed sample was mixed with carbon black in an ethanol suspension before being coated onto a glassy carbon electrode (GCE) to form the working electrode. Besides, the CV analysis was specifically conducted over a potential range of -1.0 to 1.0 V at a scanning rate of 10 mV/s.

2.4. Photocatalytic production of H_2O_2

The photocatalytic capability of TGO was evaluated for the evolution of H_2O_2 under visible light illumination, wherein the generated H_2O_2 concentration was detected through a redox reaction with iodide anion (I^-) within an acidic medium [21,22]. Particularly, 20 mg of TGO was added to a 45 mL mixture of water and IPA as the sacrificial agent with a volume ratio of 8:1 in a 100 mL beaker. The solution was subsequently irradiated under constant stirring at 200 rpm with a 50 W halogen lamb as a visible light source ($\lambda \geq 400$ nm) for 180 min, in which the light intensity and the distance to the sample were 16.67 mW/cm^2 and 5 cm, respectively. During the illumination, after each 30 min, a portion of the sample was withdrawn and filtered through a 0.22 μm nylon syringe filter to collect a transparent solution. Then, 1 mL of the filtered solution was added with 1 mL of 0.1 M KHP and 1 mL of 0.4 M KI, respectively, left for reaction at room temperature for 30 min before being quantified with UV-Vis spectroscopy at 350 nm to record the concentration of H_2O_2. Besides, the photocatalytic setup was also carried out in a tape water bath at a constant room temperature (27.8 ± 0.9 ^oC) as a control measure and was performed in triplicate to determine the average results and experimental errors.

3. RESULTS AND DISCUSSION

3.1. Characterization of materials

The functional groups arising from the surface of rGO and TGO were identified by FTIR spectra, as shown in Figure 1. Regarding the rGO, several characteristic bands can be observed at 1721, 1598, 1373, and 3326 cm^{-1}, corresponding to the oxygenated C=O, C=C,–COO, and –OH functional groups, respectively, which reveals the successful oxidation of Gi to produce GO. It is worth noting that the intensities of the signals at 1083 and 1721 cm^{-1}, derived from the stretching vibrations of C–O and C=O, respectively, are relatively low, which shows that GO has been partially reduced to rGO. In addition, simultaneous vibration bands related to the Ti–O–Ti and Ti–O–C linkages can also be detected at 600 cm^{-1}, thus confirming the successful grafting of TiO_2 onto the rGO substrate [23]. Figure 2 illustrates the XRD patterns of the two separate components and the TGO nanocomposite, in which a broad characteristic peak appears at 2θ = 25° in the diffractogram of rGO, corresponding to (002) lattice facet of the substrate, alternatively elucidating the successful reduction of GO to rGO during the hydrothermal treatment. On the other hand, regarding TiO_2, distinguished peaks located at 25.47, 37.84, 48.13, 54.01, 55.13, and 62.93° can be ascribed to the (101), (004), (200), (105), (211), and (204) crystal planes of anatase TiO_2, which eventually affirms the conversion from TIP to TiO_2 nanoparticles. Besides, the pattern of the TGO catalyst indicates notable similarities to those of the two constituents, validating the successful heterogenization of TiO_2 onto rGO sheets [24], and that is in good agreement with the FTIR spectroscopy.

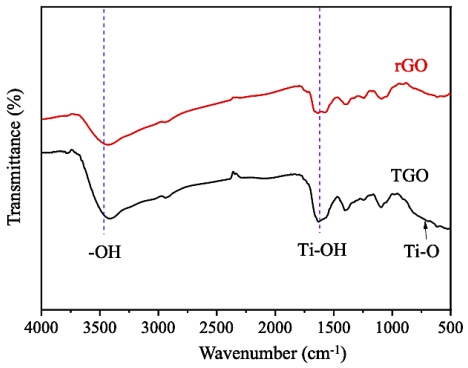

Figure 1. FTIR spectra of rGO and TGO.

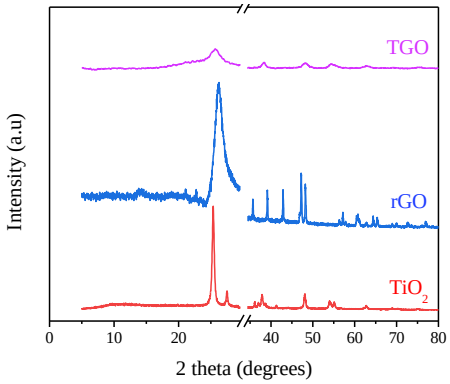

Figure 2. XRD patterns of TGO, rGO, and TiO_2.

On the other hand, the structural defects of rGO and TGO were also characterized via Raman spectroscopy, as indicated in Figure 3. For the two graphene-based materials, two dominant peaks located at ~1355 and 1615 cm^{-1} are witnessed over the recorded spectrum, which can be assigned to the D and G bands, respectively. More specifically, the former represents the characteristic vibrations of the sp^3-hybridized region, whereas the one at 1615 cm^{-1} symbolizes the resonance of sp^2 carbon atoms, corresponding to the E_{2g} phonons at the Brillouin center [25]. It is widely reported that the intensity ratio of the two mentioned peaks (I_D/I_G) can elucidate the defective degree of the carbonaceous structure, wherein a higher value would demonstrate an increase in the sp^3-domain and hence a higher degree of defects in the sample. In this case, along with a minor left-shift of the G band to 1590 cm^{-1}, the slightly higher I_D/I_G value of rGO compared to that of the incorporated TGO (1.246 versus 1.093, respectively) probably implies the impact of combining TiO_2 onto the sheet-like structure of rGO [26], resulting in the separation of graphene layers and covalent interactions of the two constituents. SEM

micrographs of rGO and TGO were contemporarily taken to evaluate the morphology of the fabricated materials (Figure 4). Accordingly, numerous folds and wrinkles can be witnessed over the surface of the rGO substrate, resulting from hydrogen bondings, π–π linkages, and Van der Waals interactions. Meanwhile, upon the introduction of TiO_2, the surface of TGO became relatively rougher which can be ascribed to the heterogenization of TiO_2 onto the rGO matrices, which consequently influenced the degree of defects in the material [27], as mentioned in the Raman spectra. Besides, multiple TiO_2 fragments with an average size of 200-400 nm can also be detected, signifying the comparably uniform distribution of the dopants throughout the profile of TGO, probably thanks to the static interaction of Ti^{4+} ions with various oxygen-containing functional groups of rGO during the chemical treatment.

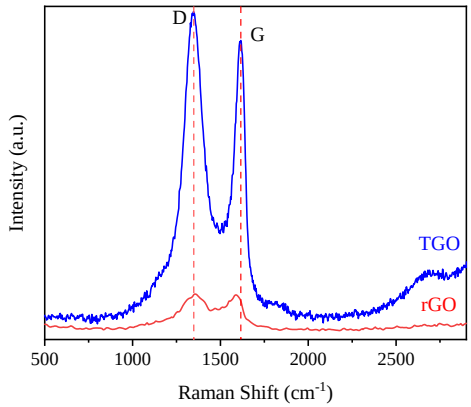

Figure 3. Raman spectra of rGO and TGO.

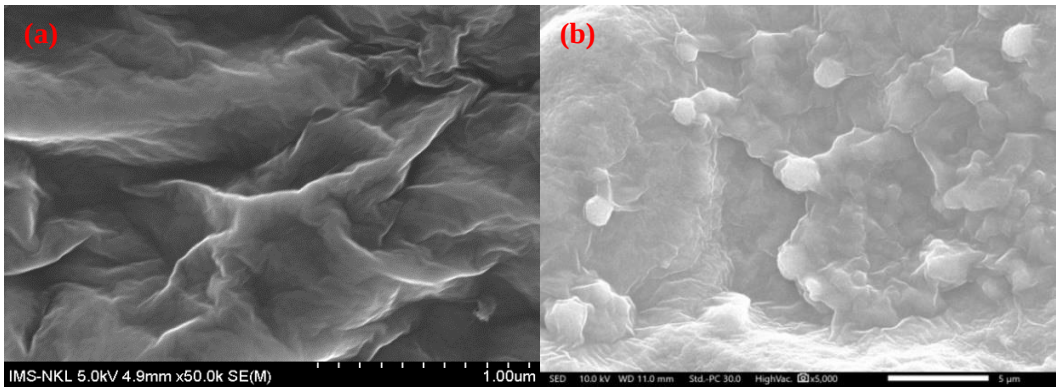

Figure 4. SEM images of (a) rGO and (b) TGO.

Furthermore, the elemental mapping of TGO was additionally recorded, indicating the uniform distribution of Ti throughout the profile (Figure 5a). Such observation suggests the successful formation of TGO with an even dispersion of TiO_2 nanoparticles throughout the graphene matrices. Meanwhile, Figure 5b validates the appearance of the three major elements, namely C, O, and Ti, in the composition of TGO via their corresponding distinct signals within the surveyed region, which confirms the formation of the composite with pure TiO_2 and rGO instead of other notable impurities. The elemental composition of the nanocomposite was also studied (Table 1).

Table 1. Elemental composition of TGO.

Element	Mass percentage (%)	Atom percentage (%)
C	35.12 ± 0.09	49.62 ± 0.12
O	38.79 ± 0.21	41.14 ± 0.22
Ti	26.09 ± 0.34	9.24 ± 0.12

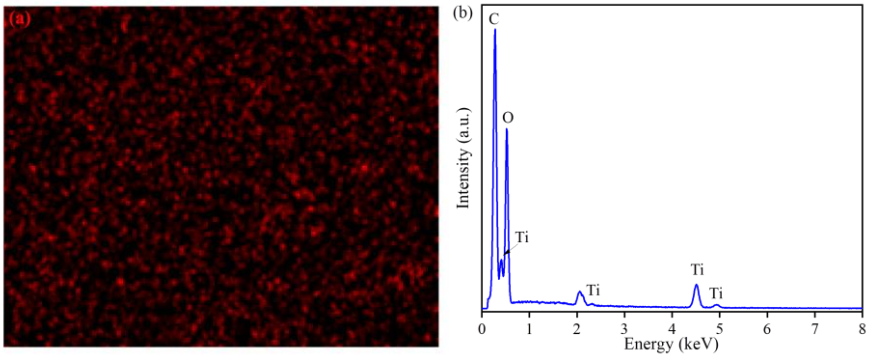

Figure 5. (a) Elemental mapping for Ti and (b) EDS spectrum of TGO.

As can be seen in Figure 6, the value of pristine TiO_2 is 3.15 eV, comparably matched with the results from previous reports [28, 29]. It is worth noting that such a relatively high band gap can limit the absorption spectrum of TiO_2 within the visible light region, which can remarkably impede the photocatalytic capability. Nonetheless, as the heterogenization between TiO_2 and rGO is introduced, the corresponding value is found to be 2.62 eV, much lower than that of bare TiO_2. Such phenomenon reveals the synergistic effects of both TiO_2 and rGO to broaden the absorption spectrum of TiO_2 [30]. More specifically, although rGO does not contribute directly to the light absorption and charge generation, the interaction of the two constituents can be anticipated to form heterojunction in the interphase [31], wherein photo-induced electrons in the valence band of rGO are excited to its conduction band, then transported to the conduction band of TiO_2. The above findings are well-accordant with some studies involving the incorporation of metallic oxide semiconductors with such graphene-like substrates [32, 33].

Further insight into the band structures of TiO_2 and TGO was additionally obtained, as calculated using Equations (1) - (3):

$$E_{VB} = \chi - E_E + \frac{1}{2}E_g \quad (1)$$

$$\chi = (\chi_i^a \times \chi_j^b \times \chi_k^c)^{\frac{1}{a+b+c}} \quad (2)$$

$$E_g = E_{VB} - E_{CB} \quad (3)$$

where E_{VB} is the valence band of the material, χ is the electron negativity of the sample, E_E is the energy of free electrons on the hydrogen scale. χ_i, χ_j, and χ_k are the energies of components i, j, and k in the material, respectively; a, b, and c are the number of molecules present for components i, j, and k of the material, respectively; and E_{CB} is the conduction band of the material.

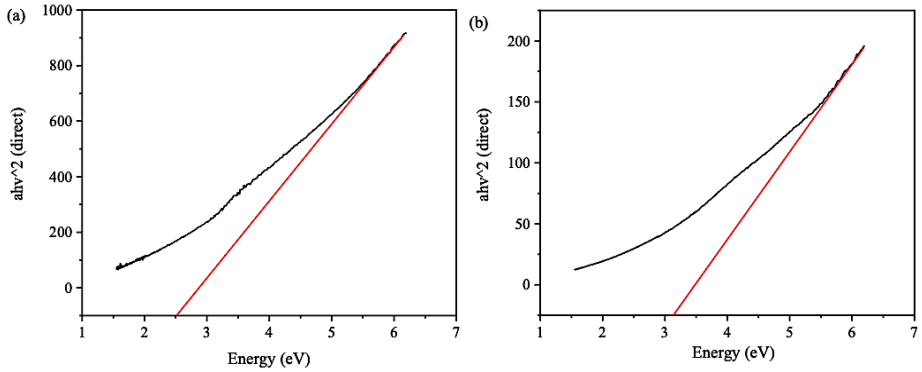

Figure 6. Band gap energies of (a) TGO and (b) TiO_2.

In detail, the valence and conduction bands of TiO_2 are determined at 2.86 and –0.29 eV, respectively [34], while the corresponding values of the nanocomposite are 3.206 and 0.586 eV, respectively. Such findings suggest that the conduction band can be dominated by the rGO constituent, which may facilitate the separation of charge carriers, as the low redox potential of rGO can act as an electron sink as well as a sacrificial site to enhance the photoactivity of the more negative conduction band of TiO_2, revealing a heterojunction and that is highly consistent with the calculated band gap energy. Moreover, some orbitals, corresponding to the minimum valence band of TiO_2, may have interacted with rGO to shift to the valence band. Therefore, the determined band structures are relatively favorable for the formation of free radicals during the photocatalysis, as the valence and conduction bands of TGO are more positive and negative than the redox potentials of $H_2O/^{\bullet}OH$ (2.28 eV) and $O_2/^{\bullet}O_2^-$ (–0.046 eV), respectively. To further validate the obtained results, the electrochemical properties of the two surveyed samples were additionally examined. Particularly, as shown in Figure 7a, EIS analysis of both TiO_2 and TGO was conducted, in which the latter exhibited a lower curve than the former. It has been extensively reported that the EIS curve can indicate the impedance of a semiconductor; herein, the impedance of TiO_2 was higher than that of TGO, confirming the advantageous influence of rGO as an electron sink to efficiently prolong the recombination of photo-induced electron-hole pairs. In addition, the CV curves of the two materials were also relatively parallelogram-shaped and redox peaks can be detected, which correlates with the electrical double-layer transportation. On the other hand, the evolution of H_2O_2, a highly essential oxidizer, has been thoroughly investigated via multiple photocatalysis processes in recent years. According to the evaluated characteristics and band structure of TGO, the photo-generation of H_2O_2 was eventually performed to investigate its catalytic performance. As can be witnessed in Figure 8, before being illuminated, a bare trace of H_2O_2 can be detected (29.96 μM), showing the vital contribution of light irradiation to the excitation and formation of radicals to produce H_2O_2. Under visible light radiation, the concentration of H_2O_2 gradually increased to 89.28 μM after 60 min before experiencing a steady increment over the remaining period, concluding at 139.73 and 158.34 μM after 120 and 180 min, respectively. This phenomenon can result from the gradual accumulation of radicals, especially reactive oxygen species (ROS), which leads to a good production rate of H_2O_2. The results obtained also reveal that the simultaneous H_2O_2 decomposition process was prevailed by the formation scheme within the examined interval. The working mechanism for H_2O_2 formation under light radiation of TGO heterojunction can be generally proposed as follows: both TiO_2 and rGO are photo-excited to generate electron-hole pairs. As demonstrated through electrochemical properties, electrons then transfer to TiO_2 while photo-induced holes

remain at the graphitic substrate, which improves the charge separation and prolongs the lifetime of charge carriers for redox reactions.

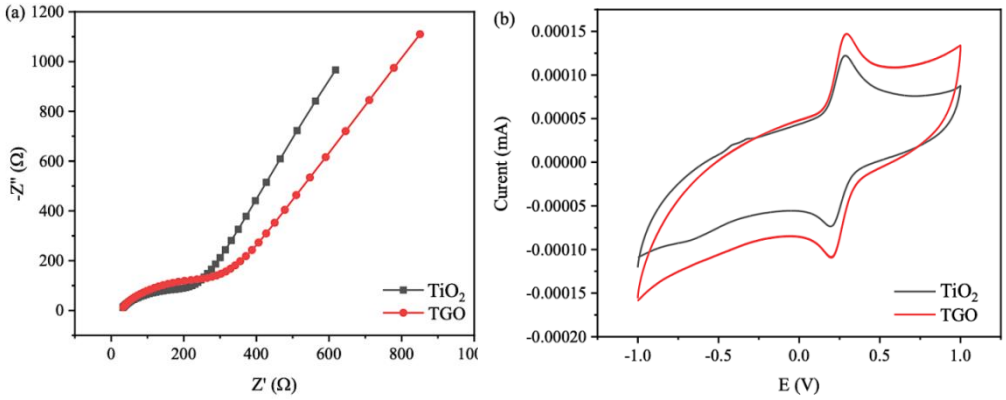

Figure 7. (a) EIS curves and (b) CV curves of TiO_2 and TGO.

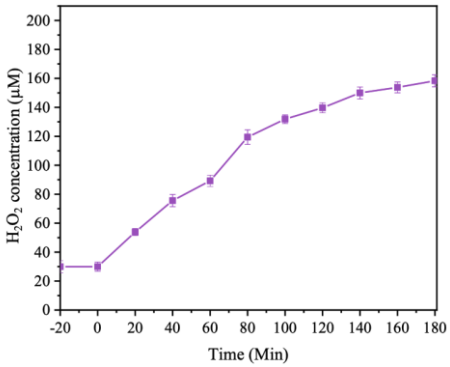

Figure 8. H_2O_2 photo-production performance of TGO.

The presence of IPA as the sacrificial agent can further prevent the electron-hole recombination via better hole scavenging activities. The combination of TiO_2 and rGO also broadens the light-responsive spectrum towards the visible light region with a lower bandgap, allowing a better photon utilization. Besides, the large surface area of rGO facilitates the essential adsorption of molecules to maximize photocatalytic interactions. Specifically, under the suitable optical band structure of TGO, secondary radicals, particularly ROS, are produced, in which hydroxyl radical ($^{\bullet}OH$) is formed based on water oxidation while the evolution of superoxide anion ($^{\bullet}O_2^-$) is related to the reduction of absorbed oxygen molecules (O_2) in the reaction medium, as illustrated in Equations (4) - (10):

$$TiO_2/rGO + h\upsilon \rightarrow TiO_2/rGO(e^- + h^+) \quad (4)$$

$$rGO(e^-) + TiO_2 \rightarrow rGO + TiO_2(e^-) \quad (5)$$

$$CH_3CH(OH)CH_3 + 2h^+ \rightarrow (CH_3)_2C{=}O + 2H^+ \quad (6)$$

$$H_2O + h^+ \rightarrow H^+ + {}^{\bullet}OH \quad (7)$$

$$O_2 + e^- \rightarrow {}^{\bullet}O_2^- \quad (8)$$

$$^{\bullet}O_2^- + 2H^+ + e^- \rightarrow H_2O_2 \quad (9)$$

$$2{}^{\bullet}OH \rightarrow H_2O_2 \quad (10)$$

The H_2O_2 photo-evolution activity of the fabricated TGO was also compared with other catalysts in several studies, as listed in Table 2. Accordingly, despite utilizing a relatively low catalyst dose (20 mg) and light source power (50 W), the TGO nanocomposite still provided a good H_2O_2 formation efficiency, reaching up to 158.34 μM after 180 min. It is noteworthy that the catalytic performance of a material is also crucially dependent on various other parameters, including the operating temperature and light source emission spectrum. Regardless, the obtained results affirm the promising applicability of TGO in several photocatalytic applications, especially the generation of H_2O_2 under light irradiation.

Table 2. H_2O_2 generation capability of several reported photocatalysts.

Material	Catalyst dose (mg)	Light power (W)	Illumination time (min)	H_2O_2 concentration (μM)	Ref.
CN/rGO@BPQDs	50	300	180	181.69	[35]
TC/pCN	50	300	60	131.71	[36]
PT-g-C_3N_4	30	300	60	27.07	[37]
TGO	20	50	180	158.34	This study

4. CONCLUSIONS

In this work, titanium dioxide-reduced graphene oxide (TGO) nanocomposite was successfully fabricated using hydrothermal method. The characterization of the as-synthesized TGO sample revealed the distinguished sheet-like structure of the rGO substrate, wherein TiO_2 nanoparticles were uniformly distributed over the graphene network and accounted for 22.89 % of the mass percentage. The recorded XRD diffractogram of the composite also provided characteristic diffraction peaks of the anatase TiO_2, validating the efficient conversion of TIP to the desired titanium dioxide constituent. Moreover, the determined valence and conduction bands of TGO were 3.206 and 0.586 eV, respectively, which is highly favorable for the separation of charge carriers and the formation of free radicals during the photocatalytic scheme. Concurrently, the photocatalytic performance of TGO was also relatively excellent with a maximum H_2O_2 concentration of 158.34 μM after 180 min under visible light illumination. Conclusively, the fabricated TGO nanocomposite possesses great potential in photocatalytic applications, particularly the evolution of hydrogen peroxide and probably the degradation of organic dyes in aqueous media.

Acknowledgments. This research is funded by Ho Chi Minh City Department of Science and Technology under grant number SVOISP-2022-KTHH-93. We acknowledge the support of time and facilities from Ho Chi Minh City University of Technology (HCMUT), VNU-HCM for this study.

CRediT authorship contribution statement. Nguyen Thanh Hoai Nam experimental, data curation and formal analysis. Che Quang Cong, Le Minh Huong writing-Original draft and Editing. Tong Hoang Lin, Nguyen Tan Thinh writing-review and editing. Doan Thi Yen Oanh, Nguyen Huu Hieu conceptualization and methodology, supervision. All authors reviewed the manuscript.

Declaration of competing interest. The authors declare that they have no known competing financial interests or personal relationships that could have appeared to influence the work reported in this paper.

REFERENCES

1. Ahmed S., Islam M. T., Karim M. A., Karim N. M. - Exploitation of renewable energy for sustainable development and overcoming power crisis in Bangladesh, Renew Energy **72** (2014) 223-235. https://doi.org/10.1016/j.renene.2014.07.003.
2. Lazarus M., Van Asselt. H. - Fossil fuel supply and climate policy: exploring the road less taken, Clim Change **150** (2018) 1-13. https://doi.org/10.1007/s10584-018-2266-3.
3. El Ouardi M., El aouni A., Ait Ahsaine H., Zbair M., Ba Qais A., Saadi M. - ZIF-8 metal organic framework composites as hydrogen evolution reaction photocatalyst: A review of the current state, Chemosphere **308** (2022) 136483. https://doi.org/10.1016/j.chemosphere.2022.136483.
4. Pasqualetti M. J. - Social Barriers to Renewable Energy Landscapes, Geographical review **101** (2011) 201-223. https://doi.org/10.1111/j.1931-0846.2011.00087.x.
5. Mulder F. M., Weninger B. M. H., Middelkoop J., Ooms F. G. B., Schreuders H. - Efficient electricity storage with a battolyser, an integrated Ni-Fe battery and electrolyser. Energy & Environmental Science **10** (3) (2017) 756-764. https://doi.org/10.1039/C6EE02923J.
6. Chen J., Symes M.D., Cronin, L. - Highly reduced and protonated aqueous solutions of 6− for on-demand hydrogen generation and energy storage, Nature chemistry **10** (2018) 1042-1047. https://doi.org/10.1038/s41557-018-0109-5.
7. Goldbach A., Bao F., Qi C., Bao C., Zhao L., Hao C., Jiang C., Xu H. - Evaluation of Pd composite membrane for pre-combustion CO_2 capture, International Journal of Greenhouse Gas Control **33** (2015) 69-76. https://doi.org/10.1016/j.ijggc.2014.12.003.
8. Wang Y., Chen B., Seo D. H., Han Z. J., Wong J. I., Ostrikov K., Zhang H., Yang H. Y. - MoS_2-coated vertical graphene nanosheet for high-performance rechargeable lithium-ion batteries and hydrogen production, NPG Asia Materials **8** (5) (2016) e268-e268. https://doi.org/10.1038/am.2016.44.
9. Cifuentes B., Bustamante F., Conesa J. A., Córdoba L. F., Cobo M. - Fuel-cell grade hydrogen production by coupling steam reforming of ethanol and carbon monoxide removal, Elsevier **43** (2018) 17216-17229. https://doi.org/10.1016/j.ijhydene.2018.07.139.
10. Iulianelli A., Basile A. - Special issue on "Hydrogen separation/purification via membrane technology", International Journal of Hydrogen Energy **45** (12) (2020) 7265-7265. doi:10.1016/j.ijhydene.2019.10.054.
11. Chen F., Dong S., Wang Z., Xu J., Xu R., Wang J. - Preparation of mixed matrix composite membrane for hydrogen purification by incorporating ZIF-8 nanoparticles modified with tannic acid, International Journal of Hydrogen Energy **45** (12) (2020) 7444-7454. https://doi.org/10.1016/j.ijhydene.2019.04.050.
12. Wornat M. J., Porter B. G., Yang N. Y. C. - Single Droplet Combustion of Biomass Pyrolysis Oils, Energy and Fuels **8** (1994) 1131-1142. https://doi.org/10.1021/EF00047A018.
13. Zaleska A. - Doped-TiO_2: A Review, Recent Patents on Engineering **2** (2008) 157-164. https://doi.org/10.2174/187221208786306289.
14. Thompson T. L., Yates J. T. - Surface Science Studies of the Photoactivation of TiO_2 New Photochemical Processes, Chemical reviews **106** (2006) 4428-4453. https://doi.org/10.1021/cr050172k.

15. Guex L. G., Sacchi B., Peuvot K. F., Andersson R. L., Pourrahimi A. M., Ström V., Farris S., Olsson R. T. - Experimental review: chemical reduction of graphene oxide (GO) to reduced graphene oxide (rGO) by aqueous chemistry, Nanoscale **9** (2017) 9562-9571. https://doi.org/10.1039/C7NR02943H.
16. Mondal A., Prabhakaran A., Gupta S., Subramanian V. R. - Boosting Photocatalytic Activity Using Reduced Graphene Oxide (RGO)/Semiconductor Nanocomposites: Issues and Future Scope, ACS Omega **6** (2021) 8734-8743. https://doi.org/10.1021/acsomega.0c06045.
17. Trinh T. T. P. N. X., Long N. H. B. S., Quang D. T., Hieu N. H. - Synthesis of graphene aerogel for adsorption of bisphenol A, In AIP Conference Proceedings **1954** (2018) 20003. https://doi.org/10.1063/1.5033383.
18. Trinh D. N., Viet T. Q. Q., Nhu T. H., Dat N. M., Thinh D. B., Hai N. D., Tai L. T., Oanh D. T. Y., Khoi V. H., Nam H. M. - Binary TiO_2/reduced graphene oxide nanocomposite for improving methylene blue photodegradation, Vietnam Journal of Chemistry **59** (2021) 395-404. https://doi.org/10.1002/vjch.202100009.
19. Viet T. Q. Q., Nhu T. H., Thinh D. B., Trinh D. N., Giang N. T. H., Dat N. M., Hai N. D., Nam H. M., Phong M. T., Hieu N. H. - Optimization of TiO_2 immobilized - Reduce graphene oxide photocatalyst toward organic compounds in aqueous medium, Synthetic Metals **280** (2021) 116867. https://doi.org/10.1016/j.synthmet.2021.116867.
20. Trinh T. T. P. N. X., Trinh D. N., Cuong D. C., Hai N. D., Huong L. M., Thinh D. B., Hoa H. N., Cong C. Q., Nam N. T. H., An H., Khoa T. D., Viet V. N. D., Phong M. T., Hieu N. H. - Optimization of crystal violet photodegradation and investigation of the antibacterial performance by silver-doped titanium dioxide/graphene aerogel nanocomposite, Ceramics International **49** (2023) 20234-20250. https://doi.org/10.1016/j.ceramint.2023.03.147.
21. Xiong J., Li X., Huang J., Gao X., Chen Z., Liu J., Li H., Kang B., Yao W., Zhu Y. - CN/rGO@BPQDs high-low junctions with stretching spatial charge separation ability for photocatalytic degradation and H_2O_2 production, Applied Catalysis B: Environmental **266** (2020) 118602. https://doi.org/10.1016/j.apcatb.2020.118602.
22. Tomita O., Otsubo T., Higashi M., Ohtani B., Abe R. - Partial Oxidation of Alcohols on Visible-Light-Responsive WO_3 Photocatalysts Loaded with Palladium Oxide Cocatalyst, ACS Catalysis **6** (2016) 1134-1144. https://doi.org/10.1021/acscatal.5b01850.
23. Lu K. Q., Xin X., Zhang N., Tang Z. R., Xu Y. J. - Photoredox catalysis over graphene aerogel-supported composites, Journal of Materials Chemistry A **6** (2018) 4590-4604. https://doi.org/10.1039/C8TA00728D.
24. Ahmadi N., Nemati A., Bagherzadeh M. - Synthesis and properties of Ce-doped TiO_2-reduced graphene oxide nanocomposite, Journal of Alloys and Compounds **742** (2018) 986-995. https://doi.org/10.1016/j.jallcom.2018.01.105.
25. Dat N. M., Cong C. Q., Hai N. D., Huong L. M., Nam N. T. H., Tinh D. Q., Tai L. T., An H., Duy M. Q., Phong M. T., Hieu N. H. - Facile Synthesis of Eco-Friendly Silver@Graphene Oxide Nanocomposite for Optical Sensing, ChemistrySelect **8** (2023). https://doi.org/10.1002/slct.202204183.
26. Zhou G., Wang D. W., Yin L. C., Li N., Li F., Cheng H. M. - Oxygen bridges between NiO nanosheets and graphene for improvement of lithium storage, ACS Nano **6** (2012) 3214-3223. https://doi.org/10.1021/nn300098m.

27. Khamboonrueang D., Srirattanapibul S., Tang I. M., Thongmee S. - TiO_2·rGO nanocomposite as a photo catalyst for the reduction of Cr^{6+}, Materials Research Bulletin **107** (2018) 236-241. https://doi.org/10.1016/j.materresbull.2018.07.002.
28. Orooji Y., Tanhaei B., Ayati A., Tabrizi S. H., Alizadeh M., Bamoharram F. F., Karimi F., Salmanpour S., Rouhi J., Afshar S., Sillanpää M., Darabi R., Karimi-Maleh H. - Heterogeneous UV-Switchable Au nanoparticles decorated tungstophosphoric acid/TiO_2 for efficient photocatalytic degradation process, Chemosphere **281** (2021) 130795. https://doi.org/10.1016/j.chemosphere.2021.130795.
29. Komaraiah D., Radha E., Sivakumar J., Reddy M. R., Sayanna R. - Photoluminescence and photocatalytic activity of spin coated Ag^+ doped anatase TiO_2 thin films, Optical Materials **108** (2020) 110401. https://doi.org/10.1016/j.optmat.2020.110401.
30. Van Bao H., Dat N. M., Giang N. T. H., Thinh D. B., Tai L. T., Trinh D. N., Hai N. D., Khoa N. A. D., Huong L. M., Nam H. M., Phong M. T., Hieu N. H. - Behavior of ZnO-doped TiO_2/rGO nanocomposite for water treatment enhancement, Surfaces and Interfaces **2**3 (2021) 100950. https://doi.org/10.1016/j.surfin.2021.100950.
31. An H., Huong L. M., Dat N. M., Hai N. D., Cong C. Q., Nam N. T. H., Tai L. T., Thi D. N. M., Nghi H. B., Huyen N. T. T., Oanh D. T. Y., Phong M. T., Hieu N. H. - Photocatalytic degradation of organic dyes using zinc oxide-decorated graphitic carbon nitride composite under visible light, Diamond and Related Materials **131** (2023) 109583. https://doi.org/10.1016/j.diamond.2022.109583.
32. Guo X., Duan J., Li C., Zhang Z., Wang W. - Highly efficient Z-scheme g-C_3N_4/ZnO photocatalysts constructed by co-melting-recrystallizing mixed precursors for wastewater treatment, Journal of Materials Science **55** (2020) 2018-2031. https://doi.org/10.1007/s10853-019-04097-0.
33. Geng X., Wang L., Zhang L., Wang H., Peng Y., Bian Z. - H_2O_2 production and in situ sterilization over a ZnO/g-C_3N_4 heterojunction photocatalyst, Chemical Engineering Journal **420** (2021) 129722. https://doi.org/10.1016/j.cej.2021.129722.
34. Gnanaseelan N., Latha M., Mantilla A., Sathish-Kumar K., Caballero-Briones F. - The role of redox states and junctions in photocatalytic hydrogen generation of MoS_2-TiO_2-rGO and CeO_2-$Ce_2Ti_3O_8$.7-TiO_2-rGO composites, Materials Science in Semiconductor Processing **118** (2020) 105185. https://doi.org/10.1016/j.mssp.2020.105185.
35. Xiong J., Li X., Huang J., Gao X., Chen Z., Liu J., Li H., Kang B., Yao W., Zhu Y. - CN/rGO@BPQDs high-low junctions with stretching spatial charge separation ability for photocatalytic degradation and H_2O_2 production, Applied Catalysis B: Environmental **266** (2020) 118602. https://doi.org/10.1016/j.apcatb.2020.118602.
36. Yang Y., Zeng Z., Zeng G., Huang D., Xiao R., Zhang C., Zhou C., Xiong W., Wang W., Cheng M., Xue W., Guo H., Tang X., He D. - Ti_3C_2 Mxene/porous g-C_3N_4 interfacial Schottky junction for boosting spatial charge separation in photocatalytic H_2O_2 production, Applied Catalysis B: Environmental **258** (2019) 117956. https://doi.org/10.1016/j.apcatb.2019.117956.
37. Lu N., Liu N., Hui Y., Shang K., Jiang N., Li J., Wu Y. - Characterization of highly effective plasma-treated g-C_3N_4 and application to the photocatalytic H_2O_2 production, Chemosphere **241** (2020) 124927. https://doi.org/10.1016/j.chemosphere.2019.124927.